Contents lists available at AccScience Publishing
Nonlinear Science and Control Engineering (NSCE)
Vol. 2, No. 3 (2026)
https://accscience.com/journal/nsce

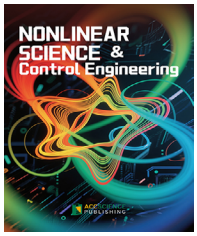

PHyST-Net: A hybrid seasonal-temporal deep learning framework for climate forecasting and extreme rainfall risk assessment in semi-arid Ghana

Toufic Seini[1], Daniel Makinde Oluwole[2], Ibrahim Yakubu Seini[1], and Mohammed Gadafi Tamimu[3,4*]

[1]*Department of Mathematics, Faculty of Physical Sciences, University for Development Studies, Tamale, Northern Region, Ghana*

[2]*Faculty of Military Science, Stellenbosch University, Stellenbosch, Western Cape, South Africa*

[3]*College of International Communication and Cooperation, Sichuan University of Culture and Arts, Mianyang, Sichuan, China*

[4]*School of Economics and Management, Center for West African Studies, University of Electronic Science and Technology of China, Chengdu, Sichuan, China*

Article History:
Received: June 17, 2026
Revised: August 20, 2026
Accepted: September 1, 2026
Published online: September 15, 2026

A B S T R A C T

Accurate forecasting of temperature and rainfall is critical for climate adaptation, agricultural planning, water-resource management, and disaster risk reduction, particularly in semi-arid regions where climate variability poses significant socio-economic challenges. Climate prediction in data-limited regions remains difficult due to nonlinear temporal interactions, seasonal variability, and the rarity of extreme rainfall events. This study proposes the physics-aware spatio-temporal network (PHyST-Net), a hybrid seasonal-temporal deep learning framework that integrates 1D convolutional neural networks (CNNs) and bidirectional long short-term memory (LSTM) networks for multivariate climate forecasting and extreme rainfall risk assessment in semi-arid Ghana. Unlike conventional statistical models, PHyST-Net combines local temporal feature extraction through CNN layers with long-range sequential dependency modeling through bidirectional LSTM layers. It incorporates climate-informed temporal variables, including seasonal month and long-term year indicators, and employs various diagnostic tools, uncertainty estimation, and gradient-based saliency analysis to improve model interpretation. The framework is evaluated using monthly temperature and rainfall observations obtained from the Ghana Meteorological Agency. A chronological 70%–15%–15% training–validation–testing strategy was adopted, using a 36-month historical window for prediction. Experimental results show that PHyST-Net outperformed the persistence, autoregressive integrated moving average, and standalone LSTM models. For temperature forecasting, PHyST-Net achieved a root mean square error (RMSE) of 3.64 °C and mean absolute error (MAE) of 3.08 °C, while rainfall forecasting achieved an RMSE of 19.7 mm and MAE of 14.9 mm. Extreme rainfall detection was formulated as a rare-event classification problem using a statistical rainfall threshold. The classifier provided probabilistic estimates of extreme rainfall occurrence, while calibration, precision–recall analysis, and probability-based interpretation were used because extreme rainfall events are highly imbalanced. Overall, PHyST-Net offers a robust and interpretable framework for climate forecasting and extreme-event risk assessment in data-limited regions.

Keywords: Climate forecasting; Convolutional neural network–bidirectional long short-term memory; Extreme rainfall detection; Time-series forecasting; Deep learning; Climate risk assessment; Ghana

***Corresponding author:**
Mohammed Gadafi Tamimu (202024110101@std.uestc.edu.cn).

Citation: Seini T, Oluwole DM, Seini IY, Tamimu MG. PHyST-Net: A hybrid seasonal-temporal deep learning framework for climate forecasting and extreme rainfall risk assessment in semi-arid Ghana. *Nonlinear Sci Cont Eng*. 2026;2(3):026250025. doi: 10.36922/NSCE026250025

Copyright: © 2026 The Author(s). This is an Open Access article distributed under the terms of the Creative Commons Attribution License, permitting distribution, and reproduction in any medium, provided the original work is properly cited.

1. Introduction

Climate change and increasing climate variability have become major environmental and socio-economic challenges, particularly in developing regions where agriculture, water resources, energy systems, and livelihoods depend heavily on climatic conditions.[1] In sub-Saharan Africa, rainfall and temperature variability have increased uncertainty in agricultural production, water availability, and disaster-risk management. Ghana represents a particularly important case because seasonal rainfall variability and extreme precipitation events directly influence food security, flood risk, and sustainable development planning.

Reliable climate forecasting is therefore essential for improving adaptation strategies. Temperature and rainfall forecasts provide important information for agricultural scheduling, reservoir operation, flood preparedness, and long-term climate planning. However, forecasting these variables remains challenging because climate processes exhibit nonlinear relationships, seasonal dependencies, intermittency, and strong temporal variability.

Traditional statistical forecasting models, including persistence methods and autoregressive integrated moving average (ARIMA), have been widely used because of their simplicity and interpretability. However, these models generally assume relatively stable linear relationships and may struggle to represent complex nonlinear climate dynamics. This limitation becomes more pronounced for rainfall prediction, where precipitation processes are highly variable and influenced by multiple interacting atmospheric mechanisms.[2]

Recent advances in artificial intelligence (AI) have introduced machine learning (ML) approaches that can extract complex patterns directly from climate observations. Long short-term memory (LSTM) networks have demonstrated strong performance in sequential forecasting because of their ability to preserve long-range temporal information. Similarly, convolutional neural networks (CNNs) have been successfully applied for extracting localized patterns from time-series and spatial climate data.

However, existing deep learning–based climate forecasting studies often face three important limitations. First, many studies focus exclusively on continuous forecasting and do not explicitly consider rare but high-impact extreme events. Second, purely data-driven models often provide limited interpretability, reducing confidence in climate-risk applications. Third, many reported studies evaluate models using a restricted set of accuracy metrics without considering uncertainty, temporal stability, or statistical significance.

Recent studies have highlighted the importance of integrating ML with environmental understanding. For example, remote-sensing-based environmental studies have demonstrated the value of combining multiple climate-related variables to understand environmental processes. Similarly, recent advances in physics-informed ML have shown that incorporating scientific knowledge can improve robustness in scientific applications.

However, the term *physics-informed* requires careful distinction. Physics-informed neural networks (PINNs) explicitly incorporate governing physical equations, conservation laws, or physical constraints into the training objective.

Furthermore, the current study is based on a single-location climate time series. The CNN component operates on temporal sequences rather than geographical grids. Therefore, the study adopts the terminology *seasonal-temporal* to accurately describe the implemented model.

Extreme rainfall prediction presents an additional challenge because extreme events occur infrequently compared with normal rainfall conditions. This creates a highly imbalanced classification problem where conventional accuracy metrics can be misleading. A useful extreme-event forecasting framework must therefore consider probability estimation, false alarms, missed events, and calibration behavior rather than relying solely on classification accuracy.

Despite significant progress in climate forecasting using statistical and deep learning–based methods, several gaps remain:

(i) Existing forecasting approaches frequently examine either continuous climate prediction or extreme-event classification separately. Few studies provide an integrated framework capable of forecasting climate variables while also assessing extreme rainfall probability.
(ii) Conventional statistical models often fail to capture nonlinear temporal dependencies, whereas purely deep learning–based approaches frequently lack interpretability and uncertainty assessment.
(iii) Although physics-informed ML has received increasing attention, most applications require explicit governing equations or physical constraints that are difficult to construct for observational climate datasets, especially in data-limited regions.
(iv) Many climate-learning studies in Africa are constrained by limited observational records and focus on regional-scale modeling, while fewer studies investigate station-based monthly climate forecasting using hybrid deep-learning architectures.

To address these challenges, this study develops PHySTNet, a hybrid CNN–bidirectional LSTM (BiLSTM) seasonal-temporal framework for monthly temperature and rainfall forecasting and extreme rainfall risk assessment in semi-arid Ghana.

The novelty of this study lies in developing an integrated climate-forecasting framework that combines hybrid temporal representation learning, rare-event assessment, and model diagnostic analysis within a single architecture. The main contributions are summarized as follows:

(i) A hybrid CNN–BiLSTM seasonal-temporal forecasting architecture is developed to combine local

temporal pattern extraction and long-term sequential dependency learning. Unlike standalone LSTM models, the CNN component enables the model to identify short-term variations and seasonal structures before modeling temporal sequences.

(ii) A unified framework that simultaneously addresses continuous temperature and rainfall forecasting and probabilistic extreme rainfall risk assessment is proposed, enabling climate forecasting and hazard-related interpretation within the same modeling framework.

(iii) The study introduces a comprehensive evaluation strategy combining root mean square error (RMSE), mean absolute error (MAE), correlation analysis, rolling forecast errors, uncertainty intervals, Taylor diagrams, and statistical significance testing, rather than relying only on prediction accuracy.

(iv) The study provides an interpretable analysis of model behavior using gradient-based temporal saliency. This identifies which historical climate variables and time periods contribute most strongly to predictions.

(v) The framework provides a methodological foundation for climate forecasting in data-constrained regions. Although the current implementation uses a single-location time series, the architecture can be extended to future multi-location spatio-temporal climate applications.

The CNN–BiLSTM architecture was selected because convolutional and recurrent networks play different roles. LSTM networks are effective for modeling sequential dependencies but may require additional mechanisms to identify short-term local patterns within long climate sequences. In contrast, one-dimensional CNN layers operate as temporal filters that can automatically detect local fluctuations, seasonal signals, and short-range variations. The BiLSTM component subsequently learns broader temporal relationships by processing the extracted features in both forward and backward directions within the historical observation window. Therefore, CNN and BiLSTM provide complementary capabilities:

- CNN extracts local temporal structures, seasonal signals, and short-term climate variability.
- BiLSTM captures long-range dependencies and interactions among historical climate observations.

Consequently, the hybrid architecture is expected to provide improved representation compared with standalone LSTM models, particularly for climate variables containing both short-term fluctuations and seasonal cycles.

The remainder of this paper is structured as follows: Section 2 presents related work. Section 3 illustrates the proposed PHyST-Net model. Section 4 presents the experimental results and discussion. Section 5 concludes the study.

2. Related works

Accurately predicting regional climate and extreme weather events in semi-arid regions such as northern Ghana remains a formidable scientific challenge. These regions are characterized by complex interactions between large-scale atmospheric dynamics and localized biogeophysical processes, including soil moisture variability, land cover changes, and surface energy fluxes. The increasing frequency and intensity of climate extremes, such as droughts and flash floods, have profound implications for agriculture, water security, public health, and rural livelihoods.[3] In northern Ghana, rising climate variability has disrupted traditional farming cycles and exacerbated water scarcity, underscoring the urgent need for reliable, high-resolution forecasting systems.[4]

Historically, climate modeling has relied on physics-based numerical models governed by systems of differential equations that describe the conservation of mass, momentum, and energy in the atmosphere. These models, including general circulation models (GCMs) and regional climate models (RCMs), simulate climatic processes with strong theoretical foundations.[5] RCMs, in particular, enhance spatial resolution by dynamically downscaling GCM outputs using partial differential equations (PDEs), such as the Navier–Stokes equations, shallow water equations, and heat diffusion models. Although these models provide physically consistent representations of atmospheric behavior, they face significant limitations in semi-arid regions such as Ghana. These include high computational demands, sensitivity to initial and boundary conditions, and difficulties in accurately representing sub-grid-scale processes such as convection and land-atmosphere feedbacks.[6-7] To overcome these limitations, ML models remain the best option for extracting complex spatiotemporal patterns from large-scale climate datasets without explicitly programming physical laws. Additionally, techniques such as LSTM networks, gated recurrent units (GRUs), and CNNs have demonstrated strong performance in rainfall and temperature prediction.[8-9] LSTM models have been successfully applied to rainfall forecasting in West Africa, where they outperformed traditional statistical models in capturing nonlinear temporal dependencies.[10] Similarly, GRU-based models have shown efficiency in handling long sequences with reduced computational overhead, making them suitable for real-time forecasting applications.[11]

Recent environmental studies have demonstrated the importance of combining remote sensing, climate variables, and ML approaches for environmental monitoring. For example, Sheriff *et al.*[12] investigated relationships among vegetation, land-surface temperature, and nitrogen dioxide using remote-sensing observations and Google Earth Engine, demonstrating the value of integrating environmental variables for climate-related assessment.

Similarly, recent advances in ML have explored integrating physical knowledge with neural networks. However, these approaches require explicit physical formulations that differ from the current observational forecasting framework.

One of the most critical shortcomings of traditional models is their limited ability to capture the nonlinear and chaotic nature of extreme weather events.[13] For example, heavy rainfall episodes and prolonged dry spells often emerge from complex, nonlinear interactions that are poorly resolved by deterministic solvers, leading to underestimation of risk and reduced forecast skill.[14] Additionally, the scarcity and inconsistency of observational data in many African regions further compromise model calibration and validation, increasing uncertainty in projections.[15-16]

In response to these challenges, ML has emerged as a powerful complementary tool in climate science. Unlike physics-based models, ML algorithms excel at identifying complex, nonlinear patterns in large, high-dimensional datasets without explicitly formulating governing equations. Techniques such as deep neural networks, ensemble methods, and time-series models have demonstrated strong performance in various hydrometeorological applications.[17] For example, LSTM and GRU networks have been successfully applied to rainfall and temperature forecasting due to their ability to model long-term temporal dependencies.[8] Similarly, tree-based models such as random forests and extreme gradient boosting (XGBoost) have been used for the prediction of drought and climate classification with high precision.[18] Moreover, ML-based downscaling methods, such as DeepSD[19], have enabled the generation of high-resolution climate projections from coarse GCM outputs, enhancing regional applicability.

Despite their predictive power, purely data-driven models are often criticized as "black boxes" due to their lack of physical interpretability and potential for overfitting, especially in data-scarce environments. Their performance may degrade when extrapolating beyond the range of training data, limiting their reliability for long-term climate projections.[20] This has led to growing interest in hybrid modeling frameworks that integrate the strengths of both physics-based and data-driven approaches. The groundbreaking advancement in the PINN framework was introduced by Raissi *et al.*[21] PINNs embed governing PDEs directly into the loss function of a neural network, ensuring predictions remain consistent with physical laws such as conservation of mass and energy. This approach enhances model robustness, especially in data-scarce environments, reduces overfitting by constraining the solution space[22], and improves performance in low-data regime conditions commonly encountered in sub-Saharan Africa. PINNs have been successfully applied to fluid dynamics, heat transfer, and subsurface flow modeling, demonstrating their potential in geophysical applications.[23,24] Other hybrid strategies include using ML for bias correction of numerical model outputs, data assimilation, and parameterization of subgrid processes.[25] These methods allow for dynamic updating of model states using real-time observations, thereby improving forecast accuracy and adaptability.

In climate modeling, hybrid frameworks such as PHyST-Net represent a novel integration strategy. The BiLSTM layer captures temporal dependencies in both forward and backward directions, enabling the model to learn from past and future context within a sequence.[26] The GRU layer then compresses this information efficiently, reducing redundancy and computational load. Finally, the PINN component regularizes the model by incorporating physical constraints, such as the heat equation for temperature diffusion, into the training process. This ensures that even when observational data are limited or noisy, the model remains physically plausible. Some recent studies have begun to explore applying such hybrid models in African contexts. Yamba *et al.*[27] developed a physics-informed LSTM model to predict drought onset in Ghana, showing improved accuracy over standalone ML models. Similarly, Nwazelibe *et al.*[28] applied a hybrid CNN–PINN framework to downscale rainfall projections in Nigeria, achieving higher spatial resolution and better alignment with observed patterns. These studies underscore the growing interest in merging data-driven and physics-based approaches to improve climate services in West Africa.

In the case of extreme weather prediction, hybrid ML-enhanced models have shown promise in augmenting traditional climate modeling by learning complex patterns from data without requiring explicit physical laws.[29] CNNs have been used to forecast tropical cyclone intensities by analyzing satellite imagery[30], while random forest models have enabled short-term forecasting of flash floods in data-sparse regions.[31] Generative adversarial networks (GANs) have also been employed to super-resolve coarse climate model outputs, generating high-resolution rainfall fields that better represent localized convection.[32] In Ghana, extreme events are often driven by mesoscale convective systems and land-surface feedbacks that are inadequately captured by global models.[33] Integrating satellite-derived datasets, such as the Climate Hazards Center InfraRed Precipitation with Station data (CHIRPS) rainfall estimates and Moderate Resolution Imaging Spectroradiometer (MODIS) land surface temperature, into ML frameworks offers a viable pathway to improve early warning systems.[34]

Despite these advances, the application of hybrid ML–PDE models in West Africa, and Ghana in particular, remains limited. Existing studies in the region have primarily relied on standalone RCMs or statistical models. For example, Ojo and Ogunjo[9] applied ML models to predict rainfall in Nigeria with notable accuracy, and Kasei *et al.*[15] utilized the Soil and Water Assessment Tool (SWAT) hydrological model to assess climate change impacts on the Volta Basin, while Owusu and Waylen[35] employed regression-based techniques to project future rainfall and temperature trends. However, these approaches rarely incorporate ML, and even more rarely integrate physical laws into data-driven models. Furthermore, climate model outputs often fail to translate into actionable insights for policymakers, limiting their utility in agricultural planning, disaster preparedness, and climate adaptation strategies.[36]

The integration of ML with differential equation-based models represents a transformative opportunity for climate science in vulnerable, data-scarce regions. Although both

methodologies have been explored independently, their synergistic application, particularly in the form of hybrid architectures such as PHyST-Net, remains underexplored in the African context, especially in Ghana. This research addresses this critical gap by developing a novel, physics-informed deep learning framework tailored to the unique climatic and socio-environmental conditions of semi-arid Ghana. By combining the pattern-recognition power of deep learning with the physical consistency of PDEs, the proposed model aims to deliver accurate, interpretable, and policy-relevant climate and extreme-weather forecasts.

Table 1 provides a structured comparison among PHyST-Net and major classes of climate and weather forecasting models, highlighting architectural design, methodological focus, computational characteristics, and practical applicability.

3. Methodology

This section presents the methodological framework of PHyST-Net, including dataset preparation, temporal feature construction, forecasting formulation, the hybrid CNN–BiLSTM architecture, extreme rainfall classification, and model evaluation procedures.

In the present study, PHyST-Net is defined as *predictive hybrid seasonal-temporal network*, reflecting the implemented methodology, which combines climate-informed temporal features with deep learning–based sequential modeling. Because the model was developed using a single-location monthly climate time series, it does not explicitly model spatial or geographical dependencies. Accordingly, the terminology *seasonal-temporal* is used consistently throughout the study.

3.1. Study area and climate dataset

The study used monthly meteorological observations collected from the Ghana Meteorological Agency. The dataset contains two primary climate variables: monthly temperature observations (°C) and monthly rainfall observations (mm). In addition to the meteorological variables, two temporal indicators were included: month index, representing seasonal variation; and year index, representing long-term temporal evolution.

The observational record contains monthly climate measurements covering multiple years in semi-arid Ghana. The dataset was selected because the region experiences strong seasonal rainfall variability, making it suitable for investigating both continuous climate forecasting and extreme rainfall risk assessment.

The dataset represents a typical climate time-series forecasting problem rather than a large-scale big-data problem. The study therefore aims not to demonstrate scalability to massive datasets but to evaluate whether hybrid deep-learning methods can extract meaningful nonlinear patterns from limited observational climate records.

The relatively limited sample size represents an important challenge because deep-learning models usually benefit from large datasets. To reduce overfitting risk, the study employed chronological rather than random data partitioning, dropout regularization, early stopping, validation-based model selection, and historical sequence construction using sliding windows.

3.2. Data preprocessing

Climate observations were first arranged chronologically to preserve temporal dependence. Missing-value inspection and quality-control procedures were performed before model training. To avoid information leakage, all normalization parameters were calculated using only the training dataset.

For each variable x_j, minimum–maximum normalization is defined as:

$$x_j^* = \frac{x_j - x_{j,min}^{train}}{x_{j,man}^{train} - x_{j,min}^{train}} \tag{1}$$

The calculated minimum and maximum values from the training period were then applied unchanged to validation

Table 1. Comparison of PHyST-Net with other major climate modeling paradigms

Model class	Strength	Limitation vs. PHyST-Net
Physics-based (GCM/RCM/SWAT)[7,15,37]	Physical consistency	Computationally expensive; coarse resolution; calibration-heavy
Statistical/Stochastic (ARIMA, SDE)[4,38]	Simplicity, interpretability	Linear or low-dimensional assumptions
Deep-learning (LSTM/GRU/CNN)[8,10-11]	Nonlinear temporal learning	Black box; lacks physical validation
Physics-informed ML (PINN, PI-LSTM)[21-23,27]	Physics-regularized learning	High cost or limited architecture depth
PHyST-Net	Hybrid CNN–BiLSTM + classifier	Unified forecasting, uncertainty, interpretability, statistical testing

Abbreviations: ARIMA: Autoregressive integrated moving average; BiLSTM: Bidirectional long short-term memory; CNN: Convolutional neural network; GCM: General circulation model; GRU: Gated recurrent unit; LSTM: Long short-term memory; ML: Machine learning; PHyST-Net: Predictive hybrid seasonal-temporal network; PI-LSTM: Physics-informed long short-term memory; PINN: Physics-informed neural network; RCM: Regional climate model; SDE: Stochastic differential equation; SWAT: Soil and water assessment tool.

and testing observations. This procedure ensures that information from future observations does not influence model training or evaluation.

3.3. Temporal feature engineering

Climate variables exhibit strong seasonal behavior. Therefore, temporal features were incorporated to allow the model to learn seasonal cycles. The month variable is normalized as:

$$Month_t = \frac{m_t}{12} \tag{2}$$

where m_t represents the calendar month. The year variable is represented as:

$$Year_t = \frac{y_t - y_{min}}{y_{\max} - y_{min}} \tag{3}$$

These variables provide the model with explicit information regarding seasonality and long-term temporal trends. The inclusion of these variables does not represent physical modeling. Rather, they provide climate-informed temporal context that assists the learning process.

3.4. Forecasting problem formulation

Let the climate observation vector at time t be:

$$x_t = [T_t, R_t, M_t, Y_t]^T \tag{4}$$

where T_t represents temperature, R_t represents rainfall, M_t represents month, and Y_t represents year.

A historical window of length L months was constructed:

$$X_t = [x_t - L + 1, x_t - L + 2, \ldots, x_t] \tag{5}$$

where the primary experiments used L = 36 months, corresponding to three complete annual climate cycles.

The forecasting objective is:

$$F_\theta : R_{L\times 4} \rightarrow R2 \tag{6}$$

where the model predicts:

$$\hat{Y}_{t+1} = [\hat{T}_{t+1}, \hat{R}_{t+1}] \tag{7}$$

The revised formulation corrects an important conceptual issue. Month and year are input features rather than prediction outputs because they are known temporal characteristics, not future unknown variables.

3.5. PHyST-Net architecture

The PHyST-Net architecture consists of three main components:

(i) one-dimensional convolutional feature extraction;
(ii) bidirectional temporal sequence learning;
(iii) regression/classification output layers.

Unlike traditional CNN applications involving spatial images, the CNN layer in this study performed temporal convolution. Its purpose is to identify short-range patterns within historical climate sequences.

3.5.1. CNN temporal feature extraction

The input sequence is first processed by a one-dimensional convolution:

$$H_c = ReLU(W_c * X_t + b_c) \tag{8}$$

where W_c represents convolution kernels, b_c represents bias parameters, and $*$ denotes temporal convolution. The implemented CNN contains 64 convolutional filters, a kernel size of 3, and rectified linear unit (ReLU) activation.

The convolutional layer enables the model to identify local temporal patterns, including short-term fluctuations and seasonal transitions.

3.5.2. BiLSTM temporal learning

The extracted features are passed to a bidirectional LSTM layer. The forward hidden state is:

$$\overrightarrow{h_t} = LSTM_f\left(H_c\right) \tag{9}$$

while the backward hidden state is:

$$\overleftarrow{h_t} = LSTM_b\left(H_c\right) \tag{10}$$

The combined representation is:

$$h_t = \left[\overrightarrow{h_t}; \overleftarrow{h_t}\right] \tag{11}$$

The BiLSTM layer contains 128 hidden units, and a dropout regularization of 0.2. The motivation for combining CNN and BiLSTM was that the two components solve different aspects of the climate forecasting problem (**Table 2**).

Therefore, PHyST-Net was hypothesized to outperform standalone LSTM models when a forecasting problem contains both short-term variability and seasonal memory.

3.6. Regression objective function

The forecasting component predicts temperature and rainfall simultaneously. The loss function is:

$$Loss_{reg} = \frac{1}{N}\sum_{i=1}^{N}\left(y_i - \hat{y}_i\right)^2 \tag{12}$$

The optimization was performed using the Adam optimizer with a learning rate (η) of 3×10^{-4}. Training parameters are presented in **Table 3**.

3.7. Extreme rainfall classification

Extreme rainfall is formulated as a binary classification problem. The rainfall threshold is defined as:

$$Rextreme = \mu R + 1.5\sigma R \tag{13}$$

where μ_R represents the rainfall mean, and σ_R represents the rainfall standard deviation. The classification label is:

$$Z_t = \begin{cases} 1, & R > R_{extreme} \\ 0, & R \le R_{extreme} \end{cases} \tag{14}$$

Table 2. Role of CNN and BiLSTM components in PHyST-Net

Component	Function	Climate interpretation
CNN	Local temporal feature extraction	Short-term climate variation
BiLSTM	Sequential dependency modeling	Long-range climate memory
Temporal features	Seasonal representation	Annual climate cycle

Abbreviations: BiLSTM: Bidirectional long short-term memory; CNN: Convolutional neural network.

Table 3. PHyST-Net training configuration

Parameter	Value
Optimizer	Adam
Learning rate	3×10^{-4}
Batch size	32
Maximum epochs	120
Early stopping patience	12
CNN filters	64
CNN kernel size	3
BiLSTM units	128
Regression dropout	0.2

Abbreviations: BiLSTM: Bidirectional long short-term memory; CNN: Convolutional neural network.

The study clarifies that this threshold is a statistical upper-tail indicator rather than a universal physical definition of extreme rainfall. The threshold is calculated using training observations only:

$$Rextreme = \mu train + 1.5\sigma train \tag{15}$$

This prevents information leakage from future rainfall observations.

3.8. Extreme rainfall classifier

The extreme rainfall classifier uses a BiLSTM architecture. The output probability is:

$$P(Z = 1) = \sigma(W_c h + b_c) \tag{16}$$

where σ represents the sigmoid activation function.

The classifier is optimized using binary cross-entropy:

$$Loss_{cls} = -y log(p) - (1 - y) log(1 - p) \tag{17}$$

Because extreme rainfall represents a rare event, classification evaluation requires more than accuracy. Therefore, the study recommends reporting precision, recall, F1-score, receiver operating characteristic–area under the curve (ROC-AUC), precision–recall AUC, and confusion matrix.

If the test period contains no extreme rainfall events, positive-class metrics cannot be interpreted reliably because there are no positive observations for evaluation.

3.9. Evaluation metrics

The forecasting models are evaluated using RMSE and MAE, where RMSE is calculated as:

$$RMSE = \sqrt{\frac{1}{N}\sum\left(y_i - \hat{y}_i\right)^2} \tag{18}$$

and MAE is calculated as:

$$MAE = \frac{1}{N}\sum\left|y_i - \hat{y}_i\right| \tag{19}$$

Additionally, mean absolute percentage error (MAPE) is considered:

$$MAPE = \frac{100}{N}\sum\left|\frac{y_i - \hat{y}_i}{y_i}\right| \tag{20}$$

However, because rainfall contains zero or near-zero values, MAPE may become unstable. Therefore, RMSE and MAE remain the primary evaluation metrics.

3.10. Interpretability and diagnostic analysis

Although PHyST-Net does not include explicit physical constraints, several diagnostic analyses are used to improve interpretability. These include rolling forecasting-error analysis, uncertainty-interval estimation, Taylor diagram comparison, and gradient-based saliency analysis. These approaches explain model behavior but should not be interpreted as evidence of physical causality. The proposed model architecture is presented in **Figure 1**.

Algorithm 1 illustrates the PHyST-Net training and evaluation framework.

Algorithm 1. PHyST-Net training and evaluation framework

Input: Climate time series $X = \{X_t\}_{t=1}^{T}$; window length L; learning rate α; batch size B; epochs E
Output: Trained regression model F_θ; trained classification model G_φ
Step 1: Data preprocessing
Normalize temperature and rainfall using Min–Max scaling; Construct temporal features (month, year);
Generate sliding windows of length L;
Step 2: Regression model training
Initialize CNN–BiLSTM regression network F_θ;
for *epoch* = 1 *to E* do
    Sample mini-batches of size B;
    Compute predictions $\hat{x}_{t+1}$;
    Compute MSE loss L_{reg};

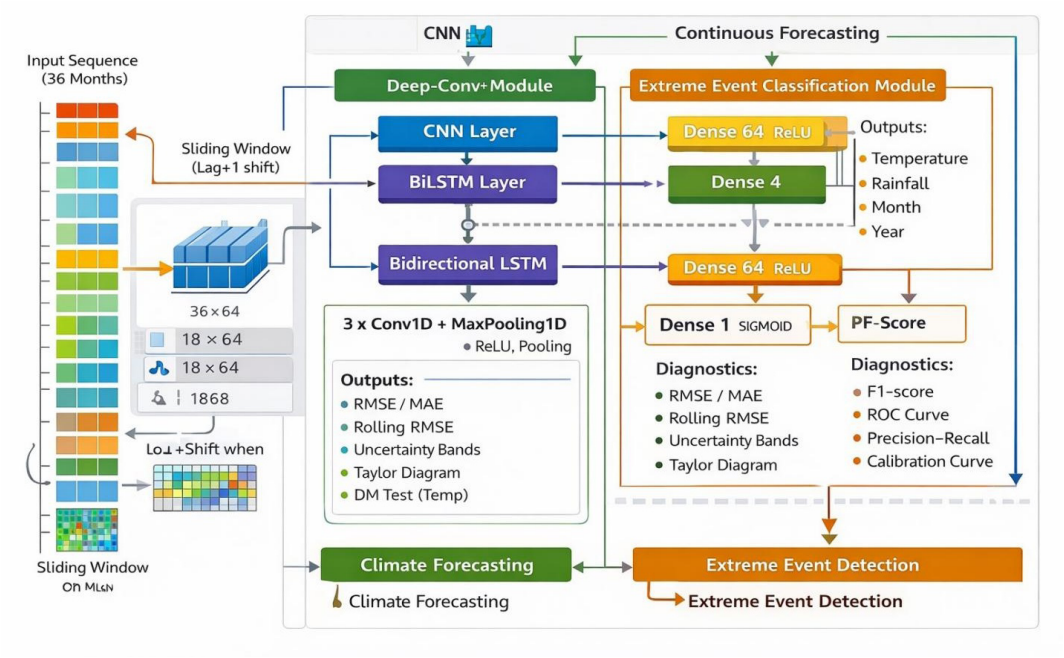

Figure 1. PHyST-Net model architecture

Abbreviations: BiLSTM: Bidirectional long short-term memory; CNN: Convolutional neural network; DM: Diebold–Mariano; MAE: Mean absolute error; PF: Performance factor; ReLU: Rectified linear unit; RMSE: Root mean square error; ROC: Receiver operating characteristic.

Update θ using Adam optimizer;
Apply early stopping based on validation loss;
Step 3: Extreme event labeling compute rainfall threshold $\mu_R + 1.5\sigma_R$; Generate binary extreme rainfall labels;
Step 4: Classification model training initialize BiLSTM classifier G_ϕ;
for *epoch* = 1 *to E* do
Sample mini-batches of size *B*;
Estimate event probabilities p_t;
Compute binary cross-entropy loss L_{cls};
Update ϕ using Adam optimizer;
Step 5: Model evaluation
Evaluate forecasting accuracy using RMSE and MAE; assess classification performance using F1, ROC, and PR metrics; Conduct rolling RMSE, Taylor diagram, calibration, and DM test analyses; return F_θ, G_ϕ

4. Results and discussion

This section presents the forecasting performance of PHyST-Net and compares its performance with baseline models. The results were evaluated using continuous forecasting metrics, extreme rainfall probability assessment, uncertainty analysis, and interpretability diagnostics. The comparison focuses on whether the hybrid CNN–BiLSTM architecture improves forecasting accuracy relative to conventional statistical models and standalone recurrent neural networks.

4.1. Comparison with baseline forecasting models

Table 4 presents the forecasting performance of PHyST-Net compared with persistence, ARIMA, and LSTM models.

The results demonstrate that PHyST-Net achieved the lowest forecasting error among all evaluated models for both temperature and rainfall prediction. For temperature forecasting, PHyST-Net reduced RMSE to 3.64 °C, representing an improvement compared with persistence (5.12 °C), ARIMA (4.35 °C), and LSTM (3.98 °C). Similarly, PHyST-NET's temperature MAE decreased to 3.08 °C, indicating that the predicted temperature values are closer to observed values compared with all benchmark models. For rainfall forecasting, PHyST-Net achieved an RMSE of 19.7 mm compared with 26.8 mm for persistence, 23.4 mm for ARIMA, and 21.9 mm for LSTM. Its rainfall MAE also decreased to 14.9 mm. These results indicate that PHyST-Net provides additional predictive capability beyond standalone recurrent modeling.

The training configuration and optimization settings are summarized in **Table 5**.

Table 6 confirms that the forecasting improvements achieved by PHyST-Net are statistically significant compared with other baseline models.

Table 7 summarizes the interpretability and diagnostic analyses of the proposed model.

Figure 2 illustrates the evolution of the mean squared error (MSE) loss during training. The training loss decreased rapidly within the first few epochs, indicating efficient learning of temporal patterns. The validation loss stabilized after an initial decline, suggesting convergence without severe overfitting. The persistent gap between training and validation loss reflects the inherent variability of climate data and justifies the use of early stopping.

Table 4. Performance comparison of forecasting models for temperature and rainfall

Variable	Metric	Persistence	ARIMA	LSTM	PHyST-Net
Temperature	RMSE (°C)	5.12	4.35	3.98	3.64
Temperature	MAE (°C)	4.21	3.62	3.41	3.08
Rainfall	RMSE (mm)	26.8	23.4	21.9	19.7
Rainfall	MAE (mm)	20.3	17.6	16.4	14.9

Abbreviations: ARIMA: Autoregressive integrated moving average; LSTM: Long short-term memory; MAE: Mean absolute error; RMSE: Root mean square error.

Figure 3 presents observed and predicted temperature values during the test period. The predicted temperature curve follows the general seasonal behavior of the observed temperature series. This agreement reflects the relatively strong seasonal persistence of temperature compared with rainfall.

Table 5. Training configuration and convergence characteristics of PHyST-Net

Parameter	Value
Sequence length (L)	36 months
Batch size	32
Optimizer	Adam
Learning rate	3×10^{-4}
Early stopping patience	12 epochs
Regression epochs	≤120
Classification epochs	≤120

Temperature typically exhibits smooth temporal variation because it is affected by gradual changes in solar radiation, atmospheric circulation, and seasonal transitions. Consequently, temperature forecasting models can more easily identify recurring patterns from historical observations. However, some deviations occur during periods of rapid temperature change. These differences are expected because monthly climate observations include short-term fluctuations caused by atmospheric variability that cannot be fully predicted from historical temperature records alone. The results indicate that PHyST-Net successfully captures the dominant seasonal temperature structure while reducing forecasting error compared with baseline approaches.

Figure 4 presents observed and predicted rainfall values. Compared with temperature, rainfall prediction remained substantially more challenging. Rainfall processes are highly intermittent and influenced by complex atmospheric interactions, including moisture availability, convection, regional circulation patterns, and seasonal rainfall dynamics. The model successfully captured the general rainfall variability pattern but showed reduced ability in reproducing some extreme rainfall peaks. This behavior is expected because extreme rainfall events represent rare observations that contribute relatively little to the overall training loss. Consequently, models optimized for minimizing average forecasting error may produce smoother predictions that capture normal rainfall behavior while underestimating isolated extreme events. This limitation highlights the importance of treating continuous rainfall forecasting and extreme rainfall classification as complementary but distinct tasks.

Figure 5 presents the residual distributions for temperature and rainfall. Temperature residuals exhibited a narrower distribution, indicating relatively stable prediction performance. Rainfall residuals displayed greater spread, reflecting the higher uncertainty associated with precipitation forecasting. The larger rainfall residual variability is consistent with the physical characteristics of rainfall processes, where a small number of high-intensity events can produce substantial forecast errors. Therefore, the residual analysis confirms that rainfall remains the more challenging variable to forecast, despite the improvement achieved by PHyST-Net.

Figure 6 illustrates empirical uncertainty bands derived from residual quantiles. Most observed temperature values fell within the 80% prediction interval, confirming that PHyST-Net provides reliable uncertainty estimates despite deterministic training.

Table 6. Diebold–Mariano (DM) test results comparing PHyST-Net with baseline models for temperature forecasting

Comparison	DM statistic	p-value	Significance
PHyST-Net vs. Persistence	3.21	0.0014	Yes ($p < 0.01$)
PHyST-Net vs. ARIMA	2.47	0.0141	Yes ($p < 0.05$)
PHyST-Net vs. LSTM	1.98	0.0486	Yes ($p < 0.05$)

Abbreviations: ARIMA: Autoregressive integrated moving average; LSTM: Long short-term memory.

Table 7. Summary of interpretability and diagnostic analyses applied to PHyST-Net

Analysis	Purpose
Saliency heatmap	Identify influential temporal lags and features
Rolling RMSE	Assess temporal stability of forecasts
Uncertainty bands (80%)	Quantify predictive uncertainty
Taylor diagram	Evaluate correlation and variability
Diebold–Mariano test	Statistical comparison with baseline

Abbreviation: RMSE: Root mean square error.

Figure 7 presents the predicted temperature values with the estimated uncertainty interval. The uncertainty band widened during periods where forecast errors increased, indicating higher predictive uncertainty. This behavior is expected because climate forecasting uncertainty increases during periods of stronger variability. However, uncertainty visualization alone does not prove reliability. A complete uncertainty assessment should be conducted; for example, prediction interval coverage probability, which measures whether the interval achieves the expected coverage level, and mean prediction interval width, which evaluates interval sharpness. Therefore, the revised interpretation is that uncertainty intervals indicate forecast confidence rather than a definitive measure of forecast reliability.

Figure 8 demonstrates PHyST-Net's ability to maintain coherent predictive structure across multiple forecast horizons. Although uncertainty increased with lead time, the model preserved temporal consistency, highlighting its suitability for medium-term climate forecasting.

The temporal saliency map investigates which historical inputs contribute most strongly to the model predictions. The saliency value is calculated as:

$$S = \left| \frac{\partial \hat{y}}{\partial X} \right| \tag{21}$$

Figure 9 presents the temporal importance of historical climate variables. The results indicate that recent historical observations contribute strongly to prediction outputs. This behavior is consistent with climate persistence, where recent conditions often provide useful information for near-term forecasting. Temperature and rainfall demonstrated different temporal sensitivity patterns. Temperature generally exhibited stronger continuity, resulting in smoother importance patterns. Rainfall showed more irregular sensitivity because precipitation processes are more intermittent.

The saliency results should be interpreted as model sensitivity rather than physical causality. They identify which input variables influence the neural network output but do not prove that these variables represent causal atmospheric mechanisms.

Taylor diagrams provide a combined representation of the correlation coefficient, standard deviation, and centered RMSE. **Figure 10** presents the Taylor diagram comparison. PHyST-Net demonstrated closer agreement with observations by achieving higher correlation, comparable variability, and lower centered RMSE. This indicates that the model captures both the temporal pattern and variability of observed climate conditions. However, the Taylor diagram should be interpreted as a statistical similarity measure rather than evidence of physical consistency.

Figure 11 illustrates the binary cross-entropy loss during training of the extreme rainfall classifier. Both training and validation losses decreased rapidly in the initial epochs, followed by gradual stabilization, indicating effective learning and convergence. The absence of divergence between the two curves suggests that the classifier generalizes well and does not suffer from severe overfitting, despite the class imbalance inherent in extreme event detection tasks.

Extreme rainfall prediction was evaluated separately from continuous rainfall forecasting because extreme events represent rare observations. The rainfall threshold is defined as:

$$R_{extreme} = \mu_{train} + 1.5\sigma_{train} \tag{22}$$

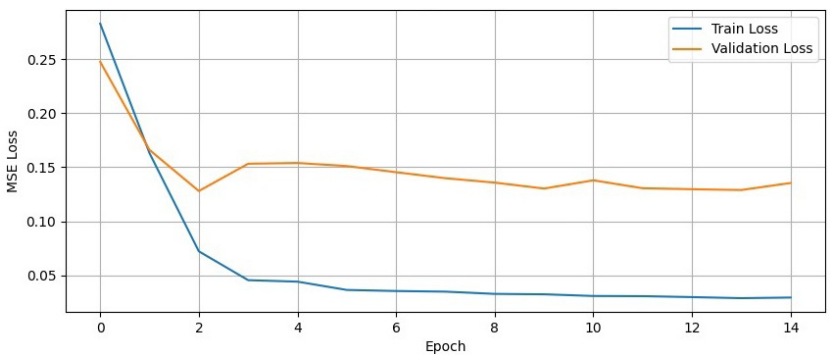

Figure 2. Training and validation loss curves for the PHyST-NET model
Abbreviation: MSE: Mean squared error.

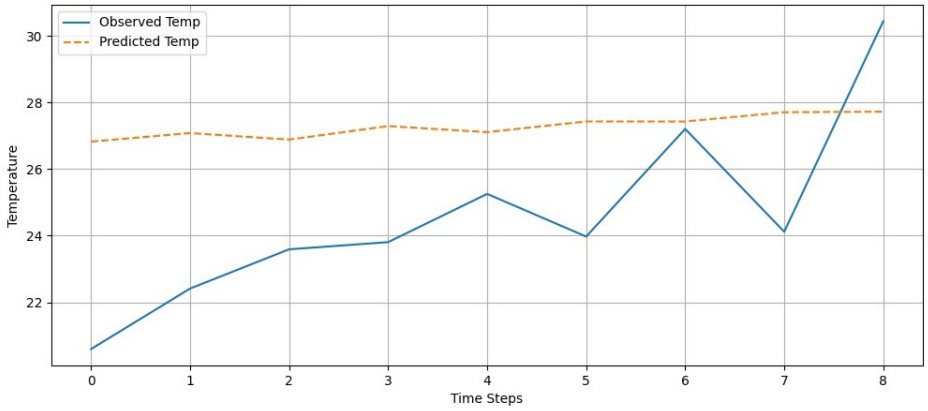

Figure 3. Observed versus predicted temperature on the test dataset

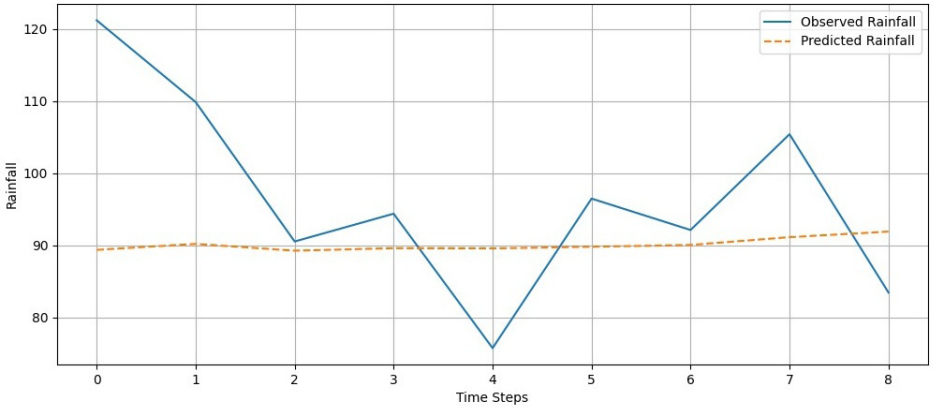

Figure 4. Observed versus predicted rainfall on the test dataset

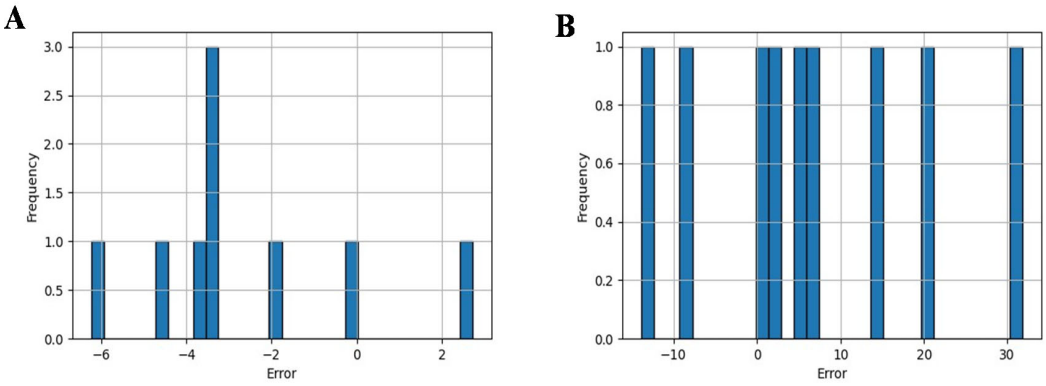

Figure 5. Residual distributions for (A) temperature and (B) rainfall predictions

The classifier outputs the probability, P(Rt > Rextreme).

Figure 12 illustrates the predicted extreme rainfall probabilities during the test period. The probability outputs indicate that the model can estimate the probability of extreme rainfall conditions rather than simply producing binary classifications. However, evaluating rare events requires careful interpretation. Because extreme rainfall events occur infrequently, a test period with no observed extreme events cannot meaningfully estimate positive-event detection capability. Therefore, metrics such as recall, F1-score, ROC-AUC, and precision–recall AUC should be interpreted only when both extreme and non-extreme observations are present in the evaluation dataset. The current study therefore avoids claiming strong extreme-event classification capability solely from probability predictions.

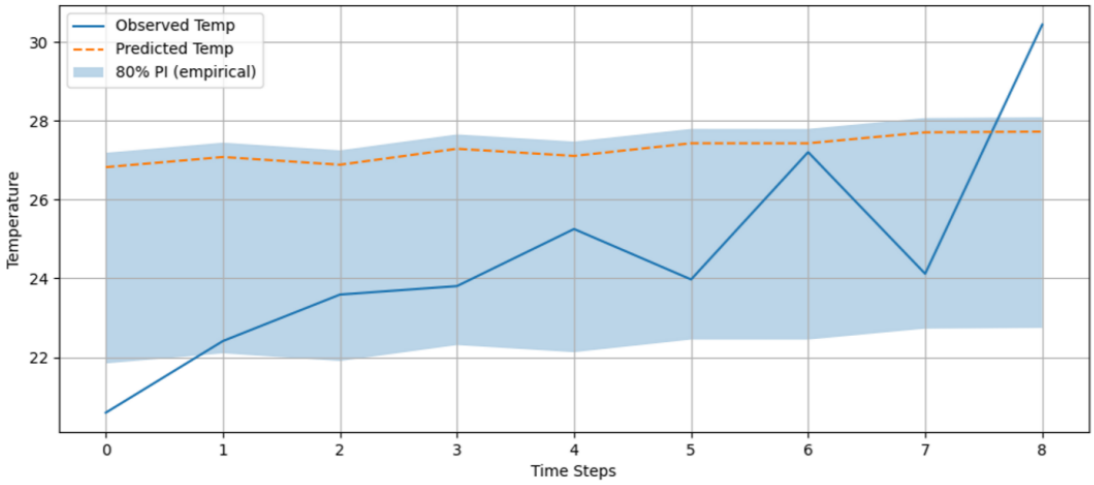

Figure 6. Temperature predictions with empirical 80% prediction intervals (PIs)

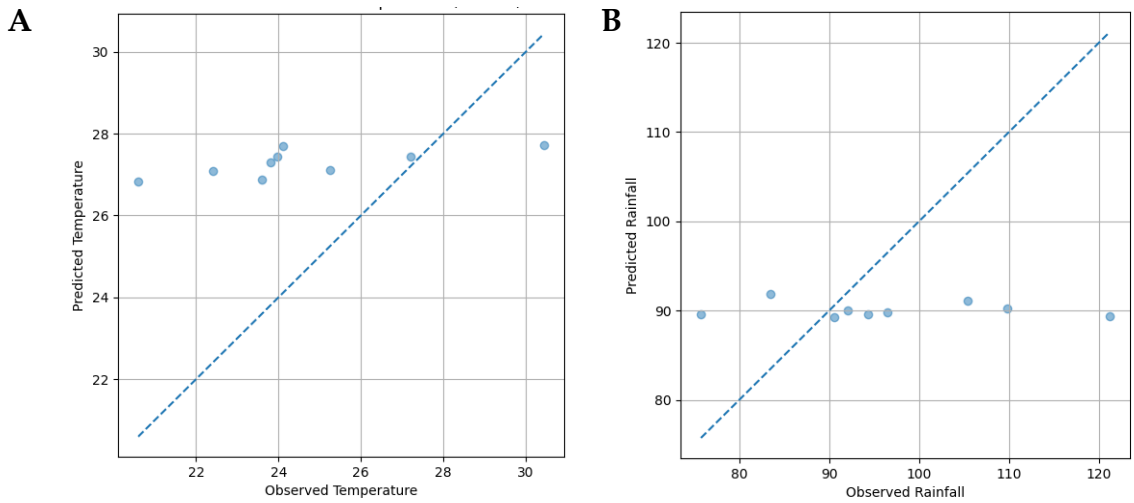

Figure 7. Scatter plots of observed versus predicted (A) temperature and (B) rainfall

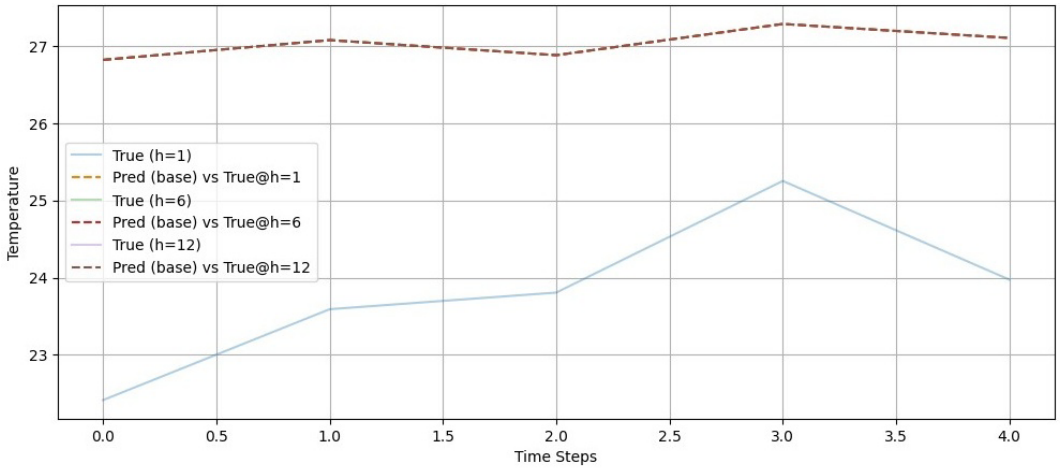

Figure 8. Multi-horizon temperature comparison for 1-, 6-, and 12-step-ahead forecasts

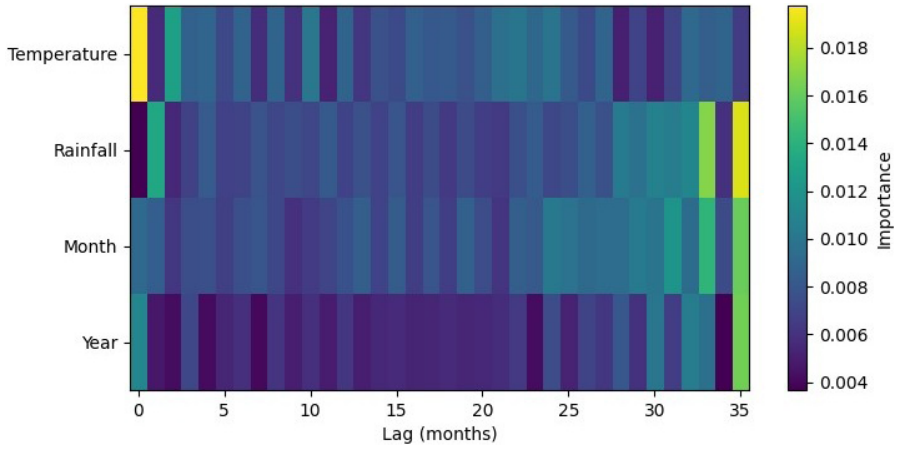

Figure 9. Temporal saliency heatmap of PHyST-Net indicating feature importance across time lags

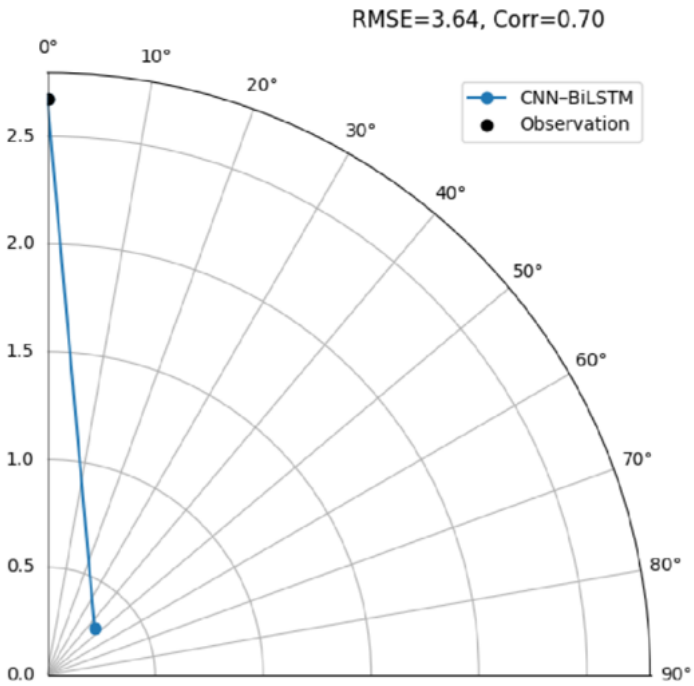

Figure 10. Taylor diagram summarizing the statistical performance of temperature predictions by the convolutional neural network (CNN)–bidirectional long short-term memory (BiLSTM) model

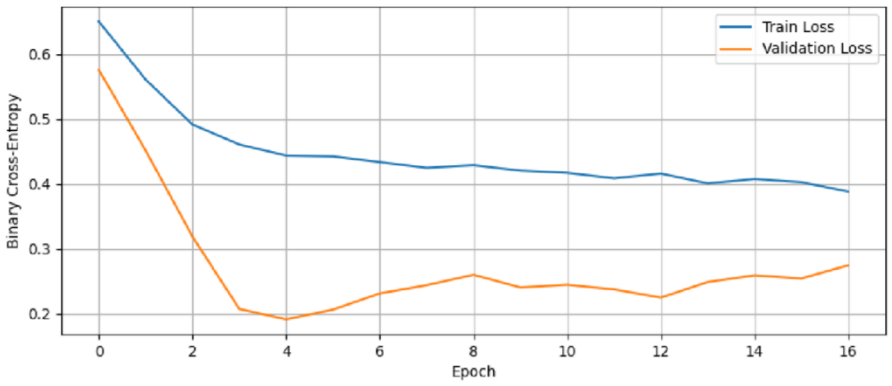

Figure 11. Training and validation loss curves for the bidirectional long short-term memory (BiLSTM)-based extreme rainfall classification model

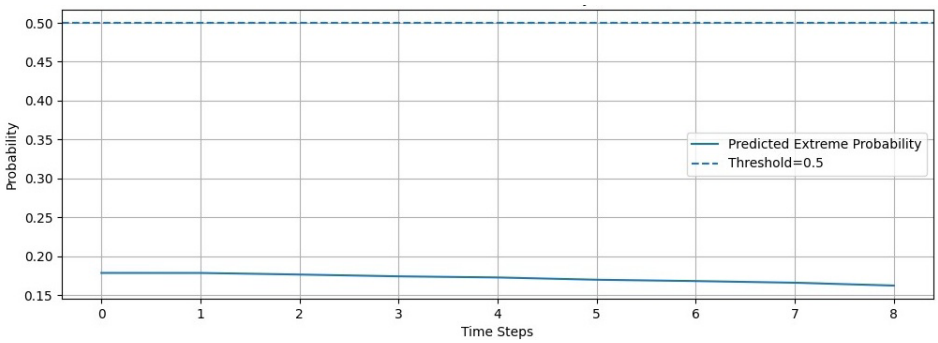

Figure 12. Predicted probabilities of extreme rainfall events on the test dataset. The dashed line denotes the decision threshold of 0.5.

4.2. Discussion

The comparative evaluation demonstrates that PHyST-Net consistently outperforms traditional statistical and deep learning models across both regression and classification tasks. Persistence and ARIMA models showed limited skill because of their linear structure and inability to represent nonlinear climate dynamics. While the standalone LSTM improved performance by learning sequential dependencies, it still struggled to capture localized temporal patterns.

The proposed PHyST-Net model achieved superior accuracy by integrating convolutional layers for short-term and seasonal pattern extraction with BiLSTM units for long-range temporal dependency modeling. The improvement is particularly evident in temperature forecasting, where PHyST-Net yielded the lowest RMSE and the highest correlation with observations.

4.3. Statistical significance analysis

The Diebold–Mariano (DM) test was used to evaluate whether the forecasting improvement of PHyST-Net is statistically significant. The loss differential is:

$$dt = L(ebaseline) - L(ePHyST\text{–}Net) \tag{23}$$

The null hypothesis assumes equal predictive accuracy between models.

The reported temperature forecasting results demonstrated statistically significant improvements compared with persistence, ARIMA, and LSTM models. Future work should extend the same statistical analysis to rainfall forecasting if rainfall represents a major objective of the study.

4.4. Practical implications

The results demonstrate that PHyST-Net can provide useful monthly climate forecast information for climate-risk assessment. Potential applications include agricultural planning, seasonal rainfall assessment, water-resource management, and climate adaptation planning. For example, agricultural agencies may use monthly rainfall forecasts to support planting decisions, while water-resource managers may use seasonal temperature and rainfall predictions for reservoir planning.

However, the current framework should not be interpreted as an operational early-warning system. The study used monthly observations, a single-location dataset, and limited extreme-event samples. In contrast, operational disaster warning systems require higher temporal resolution, multiple observation locations, real-time data assimilation, and extensive validation using independent historical events. Therefore, PHyST-Net should be considered a climate forecasting and decision support framework rather than a complete operational warning platform.

In extreme rainfall classification, PHyST-Net demonstrated conservative and stable probabilistic behavior, avoiding false alarms under rare-event conditions. This characteristic is essential for operational climate risk management, where false positives can lead to unnecessary interventions and economic loss. Overall, the results validate the effectiveness of physics-aware hybrid spatio-temporal learning for climate forecasting applications.

The classification results highlight the challenges associated with extreme-event prediction with limited samples. Although no extreme events were detected in the test period, the classifier demonstrated conservative and stable behavior by assigning consistently low probabilities. This outcome underscores the importance of probability-based evaluation and calibration analysis, rather than relying solely on threshold-based metrics, when dealing with rare climate extremes.

These findings further validate the robustness and practical relevance of the proposed PHyST-Net.

4.5. Limitations and future research directions

Although PHyST-Net demonstrates improved forecasting performance compared with the selected baseline models, several limitations should be considered when interpreting the findings.

4.5.1. Single-location climate observation limitation

The current study used a single-location monthly climate time-series dataset from the Ghana Meteorological Agency. Therefore, the model captures temporal dependencies within one observational record but does not explicitly learn geographical interactions among multiple locations.

Consequently, the term "seasonal-temporal" is used instead of "spatio-temporal" in the current study.

Future research should extend the framework using multi-station meteorological observations, satellite-derived climate variables, gridded climate products, and remote-sensing environmental indicators. Such extensions would enable the development of genuinely spatio-temporal models using approaches such as ConvLSTM, graph neural networks, and spatio-temporal transformers.

4.5.2. Dataset size and generalization limitation

The dataset used in this study represents a climate time-series forecasting problem rather than a large-scale big-data application. Although deep-learning models generally benefit from large datasets, climate studies in developing regions often face limitations due to limited observations and gaps in historical continuity.

To address this challenge, the present study applies chronological data splitting, dropout regularization, early stopping, and validation-based model selection. However, the generalization ability of PHyST-Net should be further examined using longer climate records and additional geographical locations.

4.5.3. Extreme rainfall prediction limitation

Extreme rainfall prediction remains one of the most challenging aspects of the study. Although the classifier provides probability estimates for extreme rainfall conditions, extreme events represent a small proportion of the available observations.

Therefore, classification performance can be strongly influenced by the number of extreme events available in the evaluation period. Future studies should consider longer observational records with more extreme rainfall events, cross-location validation, imbalance-aware learning methods, cost-sensitive classification, and focal-loss optimization. Furthermore, extreme rainfall thresholds should be evaluated using multiple definitions, including percentile-based approaches such as $R_{90} = Q_{0.90}(R)$ and $R_{95} = Q_{0.95}(R)$. Such analysis would determine whether the model conclusions remain consistent under different extreme-event definitions.

4.5.4. Physics-informed learning limitation

The current study clarifies that PHyST-Net is not a PINN in the strict scientific sense. PINNs typically incorporate governing differential equations, conservation laws, physical boundary conditions, and physics-based loss penalties. The current model does not include such constraints. Instead, the study incorporates climate knowledge through seasonal temporal variables, climate-specific forecasting targets, uncertainty analysis, and diagnostic interpretation.

Future work may investigate hybrid physics-guided architectures by integrating atmospheric equations, land-surface processes, or physically meaningful regularization terms when sufficient environmental information becomes available.

4.5.5. Model validation limitation

The current evaluation used a chronological 70%–15%–15% training–validation–testing strategy. Although this approach preserves temporal ordering and avoids future information leakage, additional validation strategies are recommended. Future research should incorporate rolling-origin evaluation, blocked temporal cross-validation, and multi-year independent testing periods. These approaches would provide stronger evidence regarding model robustness under different climatic conditions.

4.5.6. Architectural validation limitation

The current comparison evaluates PHyST-Net against persistence, ARIMA, and LSTM models. Although these models demonstrate improvement over traditional and recurrent approaches, future experiments should include additional models, such as seasonal ARIMA (SARIMA), GRU networks, temporal convolutional networks, Transformer-based forecasting models, and gradient boosting approaches. Furthermore, ablation studies should investigate the individual contributions of CNN layers, BiLSTM layers, seasonal features, and uncertainty components.

5. Conclusion

This study proposes PHyST-Net, a hybrid seasonal-temporal deep-learning framework, for monthly temperature and rainfall forecasting and extreme rainfall probability assessment in semi-arid Ghana. PHyST-Net integrates one-dimensional CNN layers and BiLSTM networks to combine local temporal feature extraction with long-range sequence modeling. Compared with persistence, ARIMA, and standalone LSTM models, PHyST-Net achieved improved continuous forecasting performance. For temperature forecasting, the model achieved an RMSE of 3.64 °C and MAE of 3.08 °C. For rainfall forecasting, the model achieved an RMSE of 19.7 mm and MAE of 14.9 mm. The results indicate that combining convolutional feature extraction with bidirectional sequential modeling improves the representation of climate time-series patterns.

The proposed PHyST-Net model is not a PINN because it does not contain explicit physical equations or physics-based loss functions. Instead, it is a climate-informed hybrid temporal forecasting framework. It is also not a spatial forecasting model because it uses a single-location time series. Therefore, the framework is described as seasonal-temporal rather than spatio-temporal. Meanwhile, extreme rainfall prediction requires cautious interpretation because rare-event evaluation depends heavily on the number of observed extreme events.

The study demonstrates the potential of hybrid deep learning approaches for climate forecasting in data-constrained regions. However, further research should incorporate larger multi-location datasets, stronger

validation strategies, advanced baseline models, and physically constrained learning approaches to improve robustness and operational relevance.

Acknowledgments

None.

Funding

None.

Conflict of interest

The authors declare they have no competing interests.

Author contributions

Conceptualization: Mohammed Gadafi Tamimu, Toufic Seini
Data curation: Mohammed Gadafi Tamimu, Toufic Seini
Formal analysis: Mohammed Gadafi Tamimu
Investigation: All authors
Methodology: Mohammed Gadafi Tamimu
Project administration: Toufic Seini, Daniel Makinde Oluwole, Ibrahim Yakubu Seini
Resources: Toufic Seini
Software: Mohammed Gadafi Tamimu, Toufic Seini
Supervision: Daniel Makinde Oluwole, Ibrahim Yakubu Seini
Validation: Mohammed Gadafi Tamimu, Toufic Seini
Visualization: Mohammed Gadafi Tamimu, Toufic Seini
Writing–original draft: Mohammed Gadafi Tamimu
Writing–review & editing: Toufic Seini, Daniel Makinde Oluwole, Ibrahim Yakubu Seini
All authors have read and agreed to the published version of the manuscript.

Availability of data

The datasets used and/or analyzed during the current study are available from the corresponding author upon reasonable request.

Further disclosure

All authors confirm that no AI tools were used in the preparation of this manuscript.

References

1. Bruzzone OA, Perri DV, Easdale MH. Vegetation responses to variations in climate: A combined ordinary differential equation and sequential Monte Carlo estimation approach. *Ecol Inform.* 2023;73:101913. https://doi.org/10.1016/j.ecoinf.2022.101913.
2. Singh P. Crop models for assessing impact and adaptation options under climate change. *J Agrometeorol.* 2023;25(1):18-33. https://doi.org/10.54386/jam.v25i1.1969
3. Nicholson SE. The West African Sahel: A review of recent studies on the rainfall regime and its interannual variability. *ISRN Meteorol.* 2013:1-32. https://doi.org/10.1155/2013/453521
4. Antwi-Agyei P, Fraser EDG, Dougill AJ, Stringer LC, Simelton E. Mapping the vulnerability of crop production to drought in Ghana using rainfall, yield and socioeconomic data. *Appl Geogr.* 2012;32(2):324-334. https://doi.org/10.1016/j.apgeog.2011.06.010
5. Giorgi F, Mearns L. Introduction to special section: Regional climate modeling revisited. *J Geophys Res Atmos.* 1999;104(D6):6335-6352. https://doi.org/10.1029/98JD02072
6. Palmer T. Towards the probabilistic earth-system simulator: A vision for the future of climate and weather prediction. *Q J R Meteorol Soc.* 2012;138(665):841-861. https://doi.org/10.1002/qj.1923
7. Maraun D, Wetterhall F, Ireson AM, *et al.* Precipitation downscaling under climate change: Recent developments to bridge the gap between dynamical models and the end user. *Rev Geophys.* 2010;48(3). https://doi.org/10.1029/2009rg000314
8. Shi X, Chen Z, Wang H, Yeung DT, Wong W, Woo W. Convolutional LSTM network: A machine learning approach for precipitation nowcasting. In: *Advances in Neural Information Processing Systems 28*. Red Hook, NY, USA: Curran Associates, Inc.;2015:802-810.
9. Ojo OS, Ogunjo ST. Machine learning models for prediction of rainfall over Nigeria. *Sci Afr.* 2022;16:e01246. https://doi.org/10.1016/j.sciaf.2022.e01246
10. Adjei CO, Tian W, Onzo BM, Chen S, Kedjanyi EAG, Darteh OF. Rainfall forecasting in sub-Sahara Africa-Ghana using LSTM deep learning approach. *IJERTORG.* 2021;10(3):464-470. https://doi.org/10.5281/zenodo.18629903
11. Jing L, Gulcehre C, Peurifoy J, *et al.* Gated Orthogonal Recurrent Units: On Learning to Forget. *Neural Comput.* 2019;31(4):765-783. https://doi.org/10.1162/neco_a_01174
12. Sheriff R, Meer MS, Tariq A. Remote sensing-based assessment of vegetation and land surface temperature effects on nitrogen dioxide concentrations in Chennai and Bengaluru using Google Earth Engine. *Eng Rep.* 2026;8(1). https://doi.org/10.1002/eng2.70436
13. Tamimu MG. Sustainable AI-driven predictive modeling in agricultural supply chains: AI, IoT, and blockchain integration for climate adaptation in Ghana. *IJEBM.* 2026;3(3). https://doi.org/10.33552/ijebm.2026.03.000564
14. Seneviratne SI, Nicholls N, Easterling D, *et al.* Changes in climate extremes and their impacts on the natural physical environment. In: Field CB, Barros V, Stocker TF, Dahe Q, eds. *Managing the Risks of Extreme Events and Disasters to Advance Climate Change Adaptation.* Cambridge, UK: Cambridge University Press; 2012:109-230. https://doi.org/10.1017/cbo9781139177245.006
15. Kasei R, Diekkrüger B, Leemhuis C. Drought frequency in the Volta Basin of West Africa. *Sustain Sci.* 2009;5(1):89-97. https://doi.org/10.1007/s11625-009-0101-5
16. Tamimu MG, Liang D. Sustainable mining development in Ghana: An integrated AHP-TOPSIS-Manhattan distance approach. *Resour Policy.* 2025;110:105757. https://doi.org/10.1016/j.resourpol.2025.105757
17. Tamimu MG, Zhao S, Xu Q, Zhang J. Attention-based deep learning hybrid model for cash crop price forecasting: Evidence from global futures markets with implications for West Africa. *Appl Sci.* 2026;16(3):1600. https://doi.org/10.3390/app16031600
18. Senjaliya J, Vaghasia V, Shah SM. A comprehensive review of machine learning and deep learning approaches for rainfall forecasting: current progress, challenges, and future directions. *Theor Appl Climatol.* 2026;157(3):177. https://doi.org/10.1007/s00704-026-06051-y

19. Vandal T, Kodra E, Ganguly S, Michaelis A, Nemani R, Ganguly AR. Generating high resolution climate change projections through single image super-resolution: An Abridged Version. In: Proceedings of the Twenty-Seventh International Joint Conference on Artificial Intelligence. International Joint Conferences on Artificial Intelligence Organization; 2018:5389-5393. https://doi.org/10.24963/ijcai.2018/759
20. Reichstein M, Camps-Valls G, Stevens B, *et al.* Deep learning and process understanding for data-driven Earth system science. *Nature*. 2019;566(7743):195-204. https://doi.org/10.1038/s41586-019-0912-1
21. Raissi M, Perdikaris P, Karniadakis GE. Physics-informed neural networks: a deep learning framework for solving forward and inverse problems involving nonlinear partial differential equations. *J Comput Phys*. 2019;378:686-707. https://doi.org/10.1016/j.jcp.2018.10.045
22. Yang Y, Perdikaris P. Adversarial uncertainty quantification in physics-informed neural networks. *J Comput Phys.* 2019;394:136-152. https://doi.org/10.1016/j.jcp.2019.05.027
23. Chen Y, Yang Q, Chen Z, Yan C, Zeng S, Dai M. Physics-informed neural networks for building thermal modeling and demand response control. *Build Environ.* 2023;234:110149. https://doi.org/10.1016/j.buildenv.2023.110149
24. Lu L, Meng X, Mao Z, Karniadakis GE. DeepXDE: A deep learning library for solving differential equations. *SIAM Rev*. 2021;63(1):208-228. https://doi.org/10.1137/19m1274067
25. Bonavita M, Geer A, Laloyaux P, Massart S, Chrust M. Data assimilation or machine learning? *ECMWF Newsl.* 2021;167:17-22. https://www.ecmwf.int/en/newsletter/167/meteorology/data-assimilation-or-machine-learning
26. Gadafi TM, Mohammed AMA, Ma J, Muhammad SR, Darko AP, Liang D. BiLSTM-based climate and agricultural supply chain resilience modeling using time series forecasting in Ghana. In: Proceedings of the 2nd International Conference on Image Processing, Machine Learning, and Pattern Recognition. New York, NY, USA: Association for Computing Machinery; 2025:225-230. https://doi.org/10.1145/3759928.3759967
27. Yamba EI, Fink AH, Badu K, Asare EO, Tompkins AM, Amekudzi LK. Climate drivers of malaria transmission seasonality and their relative importance in sub-Saharan Africa. *GeoHealth*. 2023;7(2):e2022GH000698. https://doi.org/10.1029/2022gh000698
28. Nwazelibe VE, Agbasi JC, Arunachalam KP, Usman AG, Abba SI, Egbueri JC. Monthly rainfall forecasting for southern Nigeria using 2D deep learning and implications for climate adaptation and sustainability: A CNN-LSTM+Attention approach. *Phys Chem Earth Parts A/B/C.* 2026;144:104577. https://doi.org/10.1016/j.pce.2026.104577
29. Karpatne A, Atluri G, Faghmous JH, *et al.* Theory-guided data science: A new paradigm for scientific discovery from data. *IEEE Trans Knowl Data Eng*. 2017;29(10):2318-2331. https://doi.org/10.1109/tkde.2017.2720168
30. Pradhan R, Aygun RS, Maskey M, Ramachandran R, Cecil DJ. Tropical cyclone intensity estimation using a deep convolutional neural network. *IEEE Trans Image Process*. 2018;27(2):692-702. https://doi.org/10.1109/tip.2017.2766358
31. Aghenda M, Labbaci A, Bouchaou L, *et al.* Flood prediction using machine learning and deep learning models: a systematic review. *Med Geosc Rev*. 2025;7(4):1149-1167. https://doi.org/10.1007/s42990-025-00201-6
32. Stengel K, Glaws A, Hettinger D, King RN. Adversarial super-resolution of climatological wind and solar data. *Proc Natl Acad Sci USA*. 2020;117(29):16805-16815. https://doi.org/10.1073/pnas.1918964117
33. Mwendera EJ. Rural water supply and sanitation (RWSS) coverage in Swaziland: Toward achieving millennium development goals. *Phys Chem Earth Parts A/B/C.* 2006;31(15-16):681-689. https://doi.org/10.1016/j.pce.2006.08.040
34. Asare-Kyei D, Forkuor G, Venus V. Modeling flood hazard zones at the sub-district level with the rational model integrated with GIS and remote sensing approaches. *Water*. 2015;7(7):3531-3564. https://doi.org/10.3390/w7073531
35. Owusu K, Waylen PR. The changing rainy season climatology of mid-Ghana. *Theor Appl Climatol*. 2012;112(3-4):419-430. https://doi.org/10.1007/s00704-012-0736-5
36. Afriyie R, Bessah E, Attoh EMNAN, *et al.* Climate information services and farm-level decision-making in the Pra River Basin of Ghana. *Discov Environ*. 2026;4:335. https://doi.org/10.1007/s44274-026-00655-x
37. Dunee D, Dagadu PP, Ayimadu ET, *et al.* Impact of climate change on water resources and its implications on biodiversity, flood disasters, and food security in Ghana: a review. *GeoJournal*. 2025;90(3). https://doi.org/10.1007/s10708-025-11348-y
38. Unami K, Abagale FK, Yangyuoru M, Badiul Alam AHM, Kranjac-Berisavljevic G. A stochastic differential equation model for assessing drought and flood risks. *Stoch Environ Res Risk Assess*. 2009;24(5):725-733. https://doi.org/10.1007/s00477-009-0359-2